A Review of Experimental Modal Analysis Methods with respect to their Applicability to Test Data of Large Aircraft Structures

Conference Paper · January 2006

Source: DLR

CITATIONS
22

READS
1,190

4 authors, including:

Yves Govers
German Aerospace Center (DLR)
69 PUBLICATIONS **242** CITATIONS

SEE PROFILE

A Review of Experimental Modal Analysis Methods with respect to their Applicability to Test Data of Large Aircraft Structures

M. Böswald, D. Göge, U. Füllekrug, Y. Govers
Deutsches Zentrum für Luft- und Raumfahrt e.V. (DLR)
Institut für Aeroelastik
Bunsenstr. 10, 37073 Göttingen, Germany
email: **marc.boeswald@dlr.de**

Abstract

In this paper, different modal analysis tools are investigated with respect to their applicability to test data from ground vibration tests (GVT) of large aircraft. Three different modal analysis methods are investigated. These are the Frequency Domain Direct Parameter Identification (FDPI), the Least-Squares Complex Exponential method (LSCE), and the Least-Squares Complex Frequency Domain method (LSCF or PolyMAX). Test data from GVT of a large aircraft usually have features like noise contamination and weak non-linearity of some modes. Thus, the influence on the results of experimental modal analysis of statistical errors (such as noise) and systematic errors (such as non-linearity) in the FRFs are investigated. Simulated FRFs of an analytical system contaminated with different levels of artificial noise are used to study the influence of statistical errors, whereas simulated non-linear FRFs obtained from an analytical system with a friction-type non-linearity is used to study the influence of systematic errors. In addition, the aforementioned modal analysis methods were applied to a dataset acquired during the GVT of the Airbus A380. The modal analysis results obtained with the different analysis methods are compared and evaluated based on the results of the analytical study of the influence of statistical and systematic errors.

1 Introduction

Ground vibration tests on aircraft prototypes are nowadays performed as a combination of the phase resonance method (sine-dwell testing) and phase separation techniques. The application of phase separation techniques has led to the requirement for reliable extraction of modal parameters such as eigenfrequencies, damping ratios, and mode shapes from a huge set of FRFs. Typically more than 500 sensors are used for GVT of modern transport aircraft. The large number of sensors together with a relatively large number of different excitation points requires efficient data management to be provided by the analysis software. Furthermore, the measured signals may be contaminated with noise as a result of long cable distances from the sensor location to the data acquisition system. In addition, some of the aircraft modes may exhibit weakly non-linear behaviour, e.g. either due to local non-linear phenomena at joints or due to the hydraulic control systems running during the test, [1].

In the past, DLR applied LMS Cada-x to extract modal parameters from FRFs measured during GVT. In particular, FDPI was found to be a reliable tool for this purpose. In the course of software improvement, Cada-x was replaced by Test.Lab where FDPI is no longer available. The Test.Lab modal analysis tools therefore had to be checked for their applicability to test data obtained from GVT of large aircraft. This was achieved by a comprehensive study performed within DLR to compare the results of three different modal analysis tools. The computational efficiency of the software when applied to a recent GVT dataset was also one of the issues to be checked. The modal analysis tools investigated were the FDPI method implemented in LMS Cada-x and the two methods available in LMS Test.Lab, i.e. the Least-Squares

Complex Exponential method (LSCE or Polyreference) and the Least-Squares Complex Frequency Domain method (LSCF or PolyMAX). The dataset used for this comparative study was obtained from the Airbus A380 GVT, because it is believed that the large number of sensors of this dataset is representative for future GVTs.

The influence of statistical errors such as noise contamination and systematic errors (e.g. due to stiffness- and damping non-linearities) were studied using an analytical 5 degree of freedom (DoF) system to assess the degree of accuracy which can be achieved for the modal parameters. Furthermore, the objective of this study was to derive basic rules to which modal analysis engineers can refer when problems come across such as high noise levels or non-linearity. These basic rules shall then indicate preferable tools which are considered to yield representative modal parameters, even in the case when the measured data reveals features which are not consistent with the assumption of linearity on which modal analysis tools are based.

2 Outline of Different Modal Analysis Tools

In the following, an outline of the theoretical background of the three modal analysis tools FDPI, LSCE, and LSCF will be described. Only some of the basic working principles will be presented for FDPI and LSCE. The LSCF theory will be presented in more detail as it is necessary for the discussion of the outcome of the studies performed in this paper.

Even though the theoretical background of the methods is quite different, they all share a common procedure for modal analysis which can be summarized in three steps. The analysis bandwidth is selected in a first step, i.e. a frequency band is cut out of the whole measured frequency range. This frequency band is considered for modal analysis and comprises a reasonable number of resonance peaks so that the model order can be kept at an acceptable level. The model order, in this respect, is the order of the equation system used for modal parameter estimation. Complex poles (i.e. eigenfrequencies and damping ratios) are estimated in a second step by analyzing the FRFs of the active analysis bandwidth according to the working principles of the different modal analysis tools. In a third step, mode shape vectors and modal scaling constants (i.e. modal mass in case of real normal modes or modal *"a"* in case of complex modes) are identified for a subset of poles selected by the operator. This third step is usually done by curve-fitting the measured FRFs while utilizing the identified eigenfrequencies and damping ratios obtained from the second step.

The identified poles usually comprise structural poles and computational poles, especially when the model order exceeds the (generally unknown) number of poles in the active analysis bandwidth. Structural poles represent structural resonances, whereas computational poles are a by-product of the specific identification algorithm and possibly noise on the data to be analyzed. The selection of meaningful poles for subsequent mode shape identification can be considered as the crucial step in modal analysis and is usually highly dependent on the experience of the operator. Tools have therefore been developed to support the selection of meaningful poles. The most commonly applied tool is the so-called stabilization diagram (e.g. see Figure 1). This is essentially a diagram in which identified poles are repeatedly plotted for different model orders used for parameter identification. Such a diagram provides quick visualization of the stability properties of identified poles. Structural poles are assumed to reappear with almost equal frequency and damping ratios, regardless of the model order. Computational poles do not have this stability property and may therefore be separated visually from the structural poles in the stabilization diagram. In principle, the stabilization diagrams work quite well, as long as the FRFs are consistent with the assumption of linearity, which real structures can only approximate. It was therefore the aim of the DLR study to find out how sensitive different modal analysis tools are with respect to weakly non-linear effects in the FRFs, because such effects are representative for data usually obtained from GVT of large aircraft structures. Such a study can effectively be carried out using simulated data where the effects of noise contamination and non-linear phenomena are known a priori.

2.1 Frequency Domain Direct Parameter Identification

The Frequency Domain Direct Parameter Identification (FDPI, see [2], [3]) operates in the frequency domain. It belongs to the group of direct methods since physical system matrices are identified in a first step and the corresponding modal parameters are calculated in a second step. The baseline of the method is the frequency domain equation of motion from which an expression for the FRF matrix can be derived:

$$\left[H(\Omega)\right] = \left(-\Omega^2\left[M\right] + j\Omega\left[C\right] + \left[K\right]\right)^{-1}. \tag{1}$$

After some algebraic transformation, and equation can be derived which is suitable for the estimation of mass modified system matrices $\left[A_0\right]$ and $\left[A_1\right]$:

$$\left(-\Omega^2\left[I\right] + j\Omega\left[A_1\right] + \left[A_0\right]\right)\left[H(\Omega)\right] = \left[B_0\right], \tag{2}$$

with:

$$\left[A_1\right] = \left[M\right]^{-1}\left[C\right],\ \left[A_0\right] = \left[M\right]^{-1}\left[K\right], \text{ and } \left[B_0\right] = \left[M\right]^{-1}. \tag{3}$$

Solving the eigenvalue problem of the mass modified system matrices yields complex eigenvalues and eigenvectors from which eigenfrequencies, damping ratios, and mode shapes can be deduced. Modal scaling constants are identified subsequently by curve-fitting the measured FRFs. An interesting feature of FDPI is that real normal modes can be obtained directly by solving the undamped eigenvalue problem using only the mass modified stiffness matrix. This is an advantage over other modal analysis method, where real normal modes are usually derived from complex ones by imposing certain assumptions.

2.2 Least-Squares Complex Exponential

Even though the Least-Squares Complex Exponential method (LSCE, see [2] and [4]) uses FRFs as an input, it essentially operates in the time domain. This is achieved by computing impulse response functions (IRFs) from the FRFs by inverse Fourier transformation. The IRFs can be expressed by a superposition of complex exponential response terms:

$$h(t) = \sum_{r=1}^{N} c_r e^{\lambda_r t} + c_r^* e^{\lambda_r^* t} = \sum_{r=1}^{2N} c_r e^{\lambda_r t}. \tag{4}$$

Each of these complex exponential response terms represents a decaying transient modal response which is a product of a time-independent residue c_r and a time-dependent complex exponential function $e^{\lambda_r t}$. The residues are local quantities and depend on the response and excitation DoFs. The complex exponential functions are global quantities and depend on the complex eigenvalues λ_r of the system. According to Prony's method, the influence of the local quantities can be separated from the influence of the global quantities so that the system poles λ_r can be calculated from the roots of the following polynomial:

$$\alpha_0 + \alpha_1 z_r + \alpha_2 z_r^2 + \cdots + \alpha_{2L} z_r^{2N} = \sum_{n=0}^{2N} \alpha_n z_r^n = 0, \tag{5}$$

where the substitutions $e^{\lambda_r \Delta t} = z_r$ and $t_n = n \cdot \Delta t$ have been introduced. In this equation, α_n are polynomial coefficients which can be identified from the IRFs according to:

$$\sum_{n=0}^{2N} \alpha_n h_n = 0, \tag{6}$$

with $h_n = h(t_n)$. Equation (6) can be established using a different set of data points $h_n, h_{n+1}, \cdots, h_{n+2N}$ and, furthermore, one can use the new data points to considerably overlap with the previous set. Accordingly, an over-determined equation system can be generated from which the polynomial coefficients α_n can be

identified in a least-squares sense. Once the polynomial coefficients α_n are identified, the z-domain poles z_r can be obtained from the roots of equation (5), and subsequently, the system poles λ_r can be deduced by applying the reverse substitution $\lambda_r = \frac{1}{\Delta t}\ln z_r$. After the system poles λ_r have been calculated, the mode shapes and modal scaling constants can be identified, either by curve-fitting the measured FRFs, or by curve-fitting the time domain impulse response functions.

2.3 Least-Squares Complex Frequency Domain

This method is commonly known as LSCF or as PolyMAX in the LMS Test.Lab environment, [5]. It uses a common denominator representation of the FRF matrix, where the FRFs are expressed by polynomial fractions with different numerator polynomials $B_{ij}(\Omega)$ depending on the respective input DoF j and the output DoF i and a common denominator polynomial $A(\Omega)$ for each FRF $H_{ij}(\Omega)$:

$$H_{ij}(\Omega) = \frac{B_{ij}(\Omega)}{A(\Omega)}. \tag{7}$$

LSCF identifies the complex polynomial coefficients of the common denominator polynomial $A(\Omega)$ and the different numerator polynomials $B_{ij}(\Omega)$ from measured FRFs $H_{ij}(\Omega)$. Instead of transforming the common denominator model (once it has been identified) into a modal model, LSCF extracts the poles of the system from the roots of the complex denominator polynomial $A(\Omega) = 0$. Subsequently, mode shapes and scaling constants are identified from curve-fitting the FRFs while the poles identified beforehand are utilized. Here, only the extraction of poles shall be discussed.

When taking into account that the FRFs are available at discrete equally spaced frequency points $\Omega_k = k\,\Delta\Omega$, $k = 0,1,\ldots,K$, and that these FRFs where obtained from time domain signals sampled at discrete time points spaced by the time increment Δt, the z-domain variable $z_k = e^{j\Omega_k \Delta t}$, $k = 0,1,\ldots,K$, can be introduced in equation (7):

$$H_{ij}(\Omega_k) = \frac{B_{ij}(z_k)}{A(z_k)}. \tag{8}$$

After some mathematical transformation, a weighted error $E_{ij}(\Omega_k)$ can be established which defines the deviation of the analytical (synthesized) FRF from the experimental ones:

$$w_{ij}(\Omega_k)E_{ij}(\Omega_k) = A(z_k)H_{ij}(\Omega_k) - B_{ij}(z_k), \tag{9}$$

$$E_{ij}(\Omega_k) = \tfrac{1}{w_{ij}(\Omega_k)}\left(A(z_k)H_{ij}(\Omega_k) - B_{ij}(z_k)\right). \tag{10}$$

Practical weighting factors $w_{ij}(\Omega_k)$ are either equal to 1 or equal to the magnitude of the FRF $w_{ij}(\Omega_k) = \left|H_{ij}(\Omega_k)\right|$ at the respective frequency point Ω_k to give the frequency points near the resonances more importance in the identification process. The polynomials $A(z_k)$ and $B_{ij}(z_k)$ are complex polynomial functions of the z-domain variable z_k with complex polynomial coefficients a_n and $b_{ij,n}$:

$$A(z_k) = \sum_{n=0}^{N} a_n z_k^n = a_0 + a_1 z_k + a_2 z_k^2 + \cdots + a_N z_k^N, \tag{11}$$

$$B_{ij}(z_k) = \sum_{n=0}^{N} b_{ij,n} z_k^n = b_{ij,0} + b_{ij,1} z_k + b_{ij,2} z_k^2 + \cdots + b_{ij,N} z_k^N. \tag{12}$$

The order N of the polynomials is the so-called model order and is related to the expected number of modes which have to be extracted from the FRFs of the current analysis bandwidth. When considering multiple FRFs from different response stations $i = 1,\ldots,I$ or respectively from different excitation positions $j = 1,\ldots,J$ then the following scalar error function can be established which summarizes the square errors between the analytical FRF of the common denominator model and the measured FRFs:

$$\varepsilon^{LSCF}\left(\{\theta\}\right)=\sum_{i=1}^{I}\sum_{j=1}^{J}\sum_{k=0}^{K}\left|E_{ij}(\Omega_k)\right|^2. \tag{13}$$

This error function is dependent on the parameter vector $\{\theta\}$ which comprises the polynomial coefficients of the numerator polynomials and the denominator polynomial:

$$\{\theta\}=\begin{Bmatrix}\vdots\\ \{\beta_{ij}\}\\ \vdots\\ \{\alpha\}\end{Bmatrix},\quad \{\beta_{ij}\}=\begin{Bmatrix}b_{ij,0}\\ b_{ij,1}\\ \vdots\\ b_{ij,N}\end{Bmatrix},\quad \{\alpha\}=\begin{Bmatrix}a_0\\ a_1\\ \vdots\\ a_N\end{Bmatrix}. \tag{14}$$

The identification of the complex polynomial coefficients is achieved by minimizing the error function defined in equation (13). When approximating this mathematical optimization problem by a first order Taylor series, a gradient based parameter estimation algorithm can be applied which can be expressed by the following equation:

$$[J]\{\theta\}=\{0\}. \tag{15}$$

Here, $[J]$ is a Jacobian matrix (gradient matrix or sensitivity matrix) containing the first order partial derivatives of the error function $\varepsilon^{LSCF}\left(\{\theta\}\right)$ with respect to the parameters comprised in $\{\theta\}$. The content of the Jacobian matrix is presented in closed form in [5] but cannot be derived here. The equation system (15) is over-determined and can be solved more efficiently by pre-multiplication with the hermitian transposed Jacobian matrix:

$$[J]^{\mathrm{H}}[J]\{\theta\}=\{0\}. \tag{16}$$

From the structure of the equation system (16) one can derive a relation between the numerator polynomial coefficients $\{\beta_{ij}\}$ and the denominator polynomial coefficients $\{\alpha\}$ by simple algebraic elimination (the exact definition of the matrix $[T_{ij}]$ is presented in [5] but cannot be derived here):

$$\{\beta_{ij}\}=[T_{ij}]\{\alpha\}. \tag{17}$$

Consequently, the parameters comprised in the parameter vector $\{\theta\}$ can be expressed by the parameters $\{\alpha\}$ by using the relations of equation (17):

$$\{\theta\}=\begin{Bmatrix}\vdots\\ \{\beta_{ij}\}\\ \vdots\\ \{\alpha\}\end{Bmatrix}=\begin{bmatrix}\vdots\\ [T_{ij}]\\ \vdots\\ [I]\end{bmatrix}\{\alpha\}. \tag{18}$$

Introducing the parameter relation stated in equation (18) into equation (16) leads to an order reduced equation system for the identification of the denominator polynomial coefficients $\{\alpha\}$:

$$[D]\{\alpha\}=\{0\}. \tag{19}$$

In order to avoid the trivial solution of equation (19), i.e. all polynomial coefficients equal to zero, a constraint has to be introduced. For example, if the polynomial coefficient a_i is set to 1, then the i-th column of the coefficient matrix $[D]$ can be separated and brought to the right hand side of the equation:

$$\underbrace{\left[\begin{array}{ccc:ccc}D_{11}&\cdots&D_{1,i-1}&D_{1,i+1}&\cdots&D_{1,N+1}\\ \vdots&&\vdots&\vdots&&\vdots\\ D_{N+1,1}&\cdots&D_{N+1,i-1}&D_{N+1,i+1}&\cdots&D_{N+1,N+1}\end{array}\right]}_{[\tilde{D}]}\begin{Bmatrix}\vdots\\ a_{i-1}\\ a_{i+1}\\ \vdots\end{Bmatrix}=-\begin{Bmatrix}D_{1,i}\\ \vdots\\ D_{N+1,i}\end{Bmatrix}. \tag{20}$$

Even though the constraint can be applied to an arbitrary coefficient, a_i, it can be shown that the introduction of this constraint has an interesting influence on the stability of the poles calculated from the roots of the denominator polynomial $A(z_k) = 0$. It is common practice to use a model order N which is typically larger than the assumed number of modes in the current analysis bandwidth. Consequently, more poles will be estimated than there are structural poles. The additional poles are called computational poles (or sometimes noise modes) and must be separated from the structural poles prior to mode shape estimation since they have no physical relevance. If the constraint is introduced on the first polynomial coefficient, i.e. $a_0 = 1$, then all other coefficients a_n can be calculated from equation (20). After the complex polynomial coefficients have been identified, the poles in the z-domain can be calculated by solving for the roots z_n of the complex polynomial:

$$a_0 + a_1 z + a_2 z^2 + \cdots + a_N z^N = 0. \tag{21}$$

The system poles can be obtained from the z-domain poles z_n by the following reverse substitution:

$$\lambda_n = \frac{1}{\Delta t} \ln z_n . \tag{22}$$

The structural poles obtained in this way (i.e. $a_0 = 1$) are stable, whereas all computational poles are unstable. Stability, in this respect, means that a pole must have positive damping. This stability effect does not occur when the constraint has been applied to another coefficient.

The stability property of the system poles obtained with $a_0 = 1$ is an interesting feature which offers the possibility to automatically remove unstable (computational) poles from the stabilization diagram. This can be considered as one of the big advantages of the LSCF method over other modal analysis methods. An example of this feature can be observed in Figure 1, where the FRFs of a 5-DoF system (see Figure 2) with 15% artificial noise on real- and imaginary part have been analyzed with an LSCF type method. The left hand side stabilization diagram shows all poles which have been calculated, whereas the unstable computational poles were automatically removed from the stabilization diagram on the right hand side.

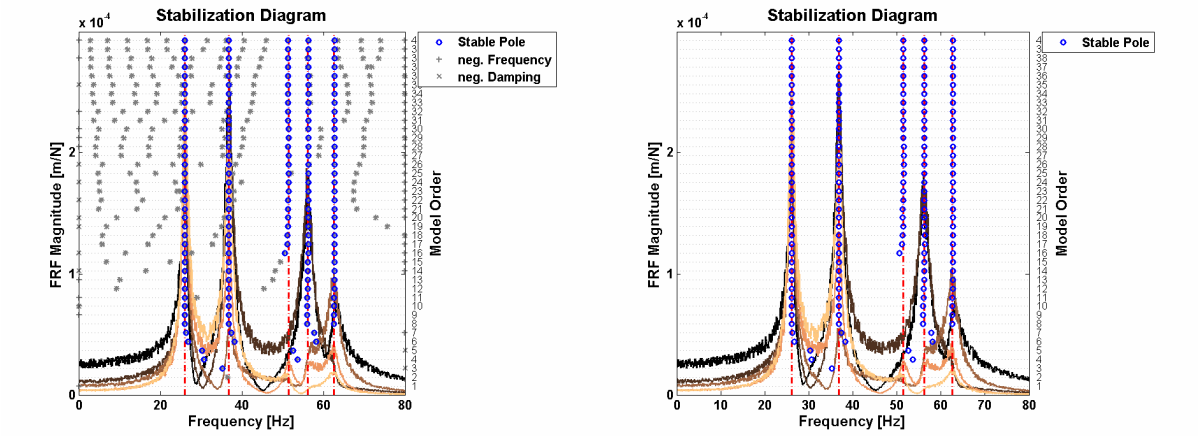

Figure 1: Stabilization diagram for 5-DoF oscillator with all poles identified (left hand side) and with unstable poles automatically removed (right hand side)

It can clearly be seen from Figure 1 that the automatic removal of unstable poles yields clear stabilization diagrams from which the structural poles can be selected conveniently. This offers efficient experimental modal analysis and also a reduction of the variability with respect to different operators of the modal analysis results, because the choice of poles is significantly reduced so that the selection of possibly wrong poles can be minimized. After the poles λ_n have been identified, the mode shapes and modal scaling constants (modal mass in case of real normal modes or modal *"a"* in case of complex modes) can be obtained by curve-fitting the measured FRFs.

3 Sensitivity with respect to Statistical Errors

During data acquisition there is always a certain amount of noise present which contaminates the measured signals. As long as the noise level is significantly lower than the level of the signals which shall be measured, it can be assumed that the influence of the noise on the modal analysis is negligible. However, in some cases the noise contamination can be significant. This can happen, for example, when long cables with poor electro-magnetic shielding are used to connect the sensors to the data acquisition system, or in the case of poor dynamic range setting of the A/D converter (underload of the digitizer) which can be a point of concern when the number of sensors is high.

In order to study the influence of noise on the modal parameter estimation process, the FRFs of the 5-DoF system shown in Figure 2 shall be analyzed. The 5-DoF system shall have the eigenfrequencies, damping ratios, and modal masses as listed in Table 1. The real normal modes of the system are shown in Table 2.

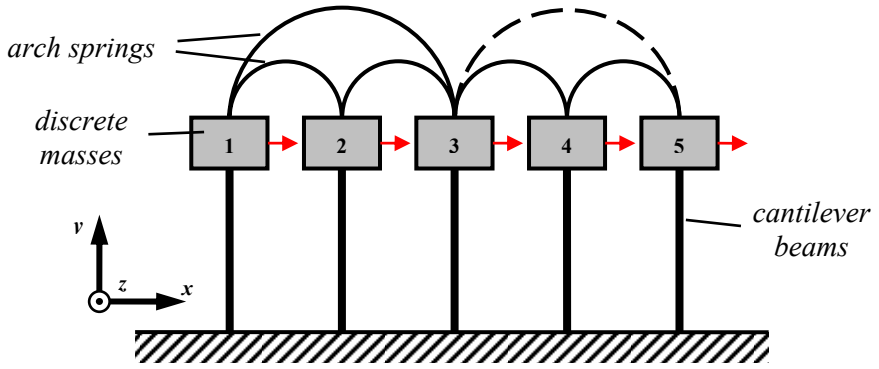

Figure 2: 5-DoF system

Table 1: Eigenfrequencies, damping ratios, and modal masses of the 5-DoF system

Mode Number	Eigenfrequ. [Hz]	Damping [%]	mod. Mass [kg m^2]
1	26,06	2	2,52
2	36,84	2	1,97
3	51,47	2	0,90
4	56,21	2	1,09
5	62,60	2	1,05

Table 2: Real normal modes of the 5-DoF system

	Mode 1	Mode 2	Mode 3	Mode 4	Mode 5
DoF 1	0,7147	1,0000	-0,0911	-0,9230	-0,6083
DoF 2	0,7166	0,9999	-0,1493	1,0000	-0,1937
DoF 3	0,7981	0,2257	0,1554	-0,1518	1,0000
DoF 4	0,8518	-0,5166	1,0000	0,1231	-0,3936
DoF 5	1,0000	-0,8590	-0,5860	0,0196	-0,2041

Different modal analysis methods were used to analyze the first column of the FRF matrix of the 5-DoF system (i.e. excitation at DoF 1, response at DoFs 1 to 5) with different levels of artificial noise, amongst 1%, 2.5%, 5%, 10%, 15%, and 25%. The noise consists of uncorrelated white noise which has been added to the real- and the imaginary parts of the FRFs independently. The pure analytical FRFs which were contaminated with noise were calculated in the frequency range from 0 to 80 Hz with a frequency resolution of 0.1 Hz. Figure 3 shows the drive point FRF with a level of 10% and 25% additional noise to illustrate the effect of noise contamination. It can be seen that a noise level of 25% is rather excessive, whereas noise levels of approximately 10% (such as shown in Figure 3) can be considered representative

for the FRFs acquired during GVT of large aircraft (e.g. due to long cable distances and poor dynamic range settings of the A/D converter).

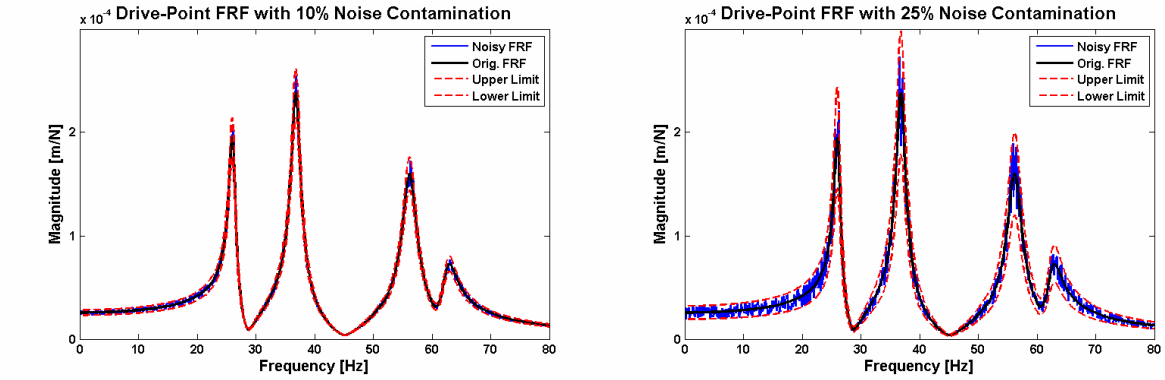

Figure 3: Noise contaminated drive point FRF with 10% and 25% artificial noise

As a first check, modal analysis was carried out on the analytical (simulated) FRFs without noise contamination using all three analysis methods (FDPI, LSCE, and LSCF). As expected, all methods identified the modal parameters from the FRFs with deviations in frequency and damping smaller than 0.01%.

Prior to the discussion of the accuracy of modal parameter extraction from noisy data, the influence of noise on the stabilization diagrams of the different methods will be discussed. Therefore, the stabilization diagrams obtained when analyzing the FRFs with 15% noise will be used to illustrate the effects of noise on the pole estimation. Figure 4 shows the stabilization diagram obtained with the Cada-x implementation of FDPI. It can be observed that the analysis bandwidth of 20 to 70 Hz does not yield stable poles for the higher modes due to the noise. In addition, the diagram looks somewhat fuzzy because of the computational poles which appear between the first and the second resonance peak. Nonetheless, after dividing the frequency range into a lower (20 to 45 Hz) and an upper (45 to 70 Hz) analysis bandwidth, all modes stabilized in the stabilization diagram and could therefore be extracted from the noise-contaminated FRFs. The computational poles between the first and the second resonance peak also appeared after the analysis bandwidth was narrowed down. The selection of meaningful poles for subsequent mode shape identification can thus not be done in an automated way. Instead one has to take a close look in order to avoid the selection of a wrong (computational) pole.

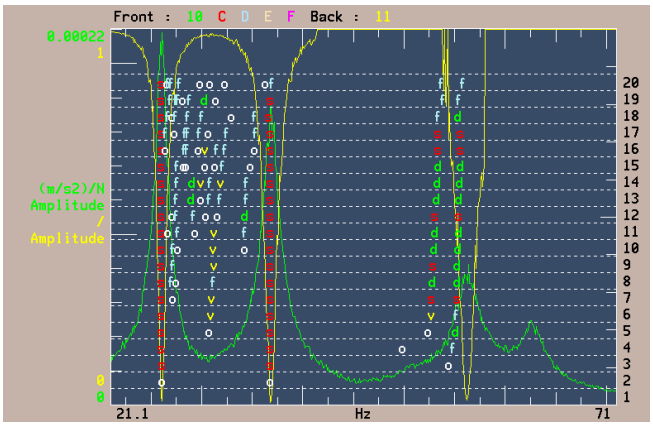

Figure 4: Stabilization diagram obtained with FDPI for 15% artificial noise

Figures 5 and 6 show the stabilization diagrams obtained with the Test.Lab implementation of LSCE and LSCF, respectively. Both methods can extract the modes out of the broad analysis bandwidth from 20 to 70 Hz. Even though both methods achieved stability for all structural poles, additional stable (computational) poles can be observed in the LSCE stabilization diagram as a result of additional noise. These make the diagram look somewhat fuzzy.

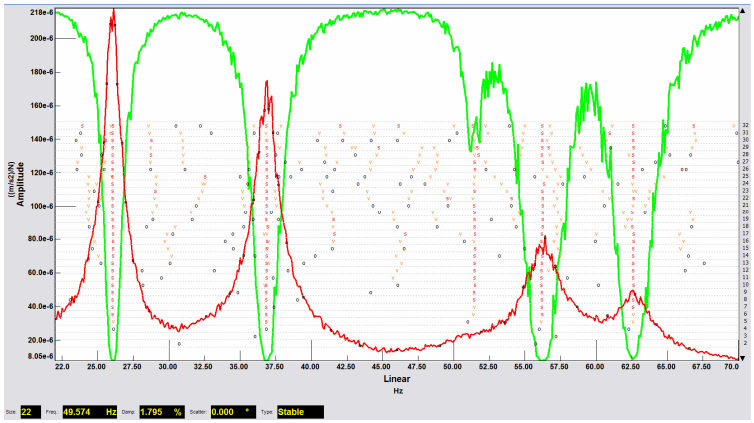

Figure 5: Stabilization diagrams obtained with the Test.Lab implementation of LSCE

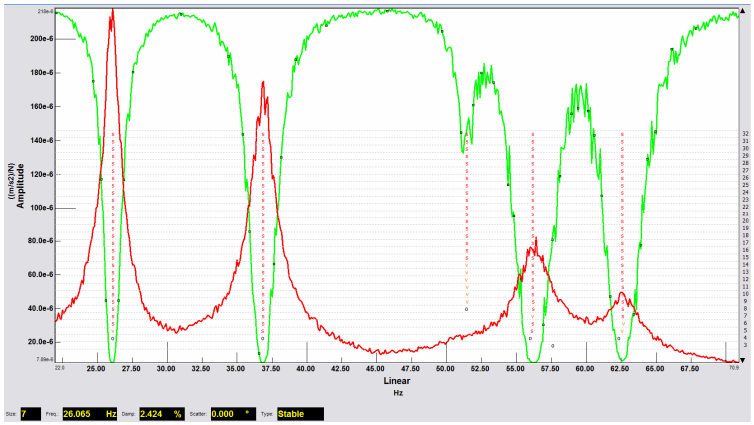

Figure 6: Stabilization diagrams obtained with the Test.Lab implementation of LSCF

In principle, LSCF estimates as many poles as LSCE. The advantage of LSCF is that only the structural poles have positive damping, whereas the computational poles appear with negative damping and can thus be removed automatically from the stabilization diagram. This is a very convenient feature, because it makes it easier to select (meaningful) poles from the stabilization diagram for subsequent mode shape identification. Moderate noise levels do not affect the visual appearance of the stabilization diagram of LSCF as a result of this feature.

The errors of the identified eigenfrequencies and damping ratios of the different modes will be discussed next. The modal analysis was performed in a bandwidth from 20 to 70 Hz. This frequency range was analyzed in one step by LSCE and LSCF but had to be divided into two analysis bandwidths (20 to 45 Hz and 45 to 70 Hz) for FDPI. It is sufficient here to focus the discussion on the first three modes, because the results of the other two modes showed similar characteristics. It should be mentioned that the first two modes are excited quite well from the drive point (DoF 1), whereas mode 3 is poorly excited in this case. This is confirmed by the sum FRF (summation of all FRFs, red curve) and the mode indicator function (green curve) plotted in the stabilization diagrams of Figure 5.

Modal analysis was performed using the FRFs contaminated with six different levels of artificial noise (1%, 2.5%, 5%, 10%, 15%, and 25%). The FRFs of each noise level were analyzed using three different methods (FDPI, LSCE, and LSCF). The eigenfrequency- and damping errors are plotted as functions of the noise level in order to visualize possible relations among the noise level and the frequency- and damping error. Figures 7 and 8 show the eigenfrequency- and damping errors of modes 1, 2, and 3. It can be seen that the eigenfrequencies can be extracted with relatively good accuracy with all three analysis methods, regardless of the noise level. Indeed, the largest eigenfrequency error is only -0.4% and was obtained with FDPI for the second mode at the highest noise level. The damping error is generally more pronounced and it can be seen that LSCF yields the poorest damping estimates. Damping is underestimated by LSCF and this situation becomes worse when the noise level is increased. This can be

observed from the damping errors plotted in Figures 7 and 8 for all three modes. It should be noted that the damping error associated with the poorly excited mode 3 is about -83% for the highest noise level which is far away from the damping estimates of LSCE and FDPI.

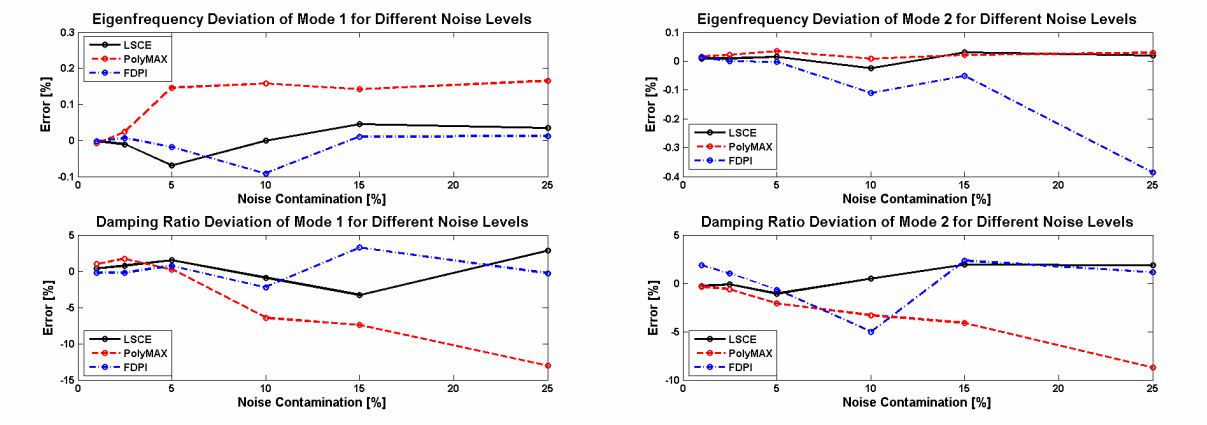

Figure 7: Error of identified eigenfrequencies and damping ratios of modes 1 and 2 for different noise levels

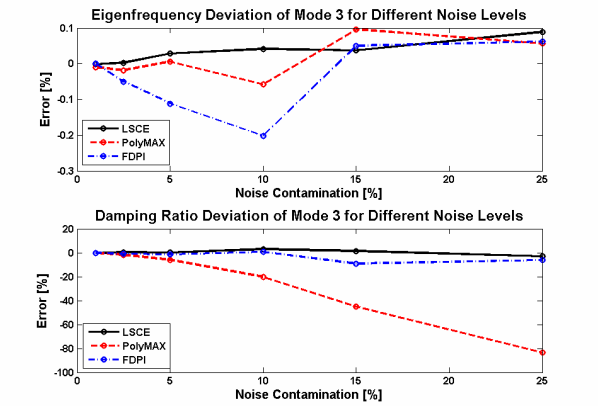

Figure 8: Error of identified eigenfrequency and damping ratio of mode 3 for different noise levels

The errors in the mode shapes were negligible and shall therefore not be discussed here. In fact, mode shapes are identified by curve-fitting the noisy FRFs in a least-squares sense, thereby eliminating the effect of white noise. In addition, mode shapes are relative quantities which are typically less sensitive to errors in the global damping estimate. Nonetheless, complex modes may appear more complex when damping was significantly over-estimated. Errors of the modal scaling constants (i.e. modal mass or modal *"a"*) with respect to noise levels were not considered. However, these quantities are also obtained from curve-fitting the FRFs and are generally much more sensitive to errors in the global damping estimates than to noise. One can refer to a rule of thumb which states that too high a damping estimate yields too low a modal mass and vice versa. As an illustration of this rule the curve-fit of the drive point FRF of the 5-DoF system is shown Figure 9 with a relatively high level of noise (15%). An error of +50% was intentionally imposed on the damping ratio of mode 1 prior to curve-fitting. The curve-fit was performed in the frequency range from 20 to 70 Hz (no weighting) and it can be seen that the curve-fit at the resonance of mode 1 is not very good. Consequently, the modal mass was identified with an error of -26.6%. In addition, the modal mass was slightly complex after identification. Nonetheless, the real normal mode shape was still identified with acceptable accuracy, i.e. the maximum error of a vector component is -5.1% for the drive point DoF and the MAC value between the identified mode and the analytical mode was 99.96%. It should also be mentioned that the error in the damping estimate of the (well excited) mode 1 yields a significant error in the modal scaling constant of the poorly excited mode 3 of +31.3%. Even in case of noise-free FRFs, the +50% error of the damping of mode 1 yields an error of

-20.8% in the modal mass of that mode, but more importantly, an error of +51.2% in the modal mass of the poorly excited mode 3. Thus, modal scaling constants of poorly excited modes cannot be considered reliable since they can be highly dependent on the damping estimates of other modes in the analysis bandwidth.

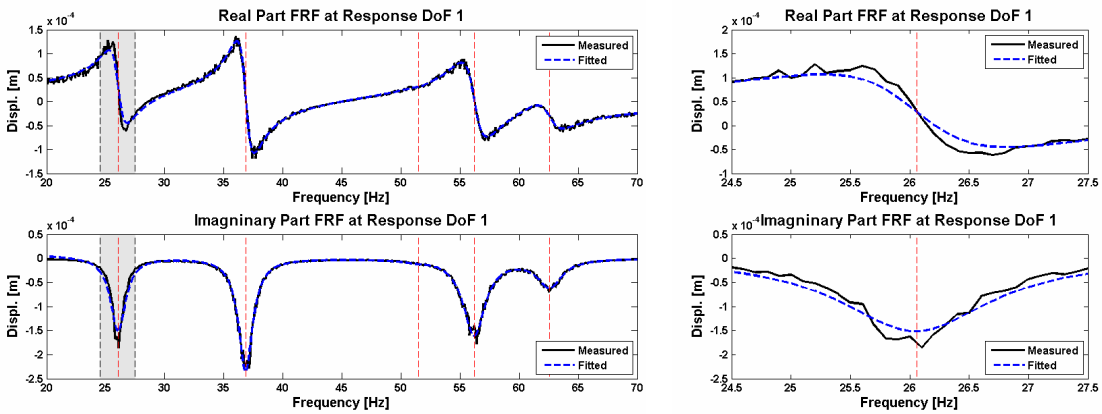

Figure 9: Overall curve-fit of drive point FRF of 5-DoF system with 50% error on the damping ratio of the first real normal mode and zoomed curve-fit in the vicinity of the resonance of mode 1

As a conclusion of the results of the study of the different modal analysis methods with respect to their sensitivity to statistical errors such as noise on the FRFs, it should be mentioned that in case of significantly noisy data it is sometimes worth to check the results of different methods against each other. More convenient methods are not necessarily more accurate in any case, even though one might get that impression from the clear stabilization diagrams. Even though eigenfrequencies and mode shapes can be extracted quite accurately from noisy FRFs, it has to be mentioned that the damping estimates are typically less accurate. The best way to check the quality of the damping estimates is from the quality of the curve-fit of the synthesized FRFs with the measured ones.

When looking at the damping estimates from the LSCF analysis as a function of the noise levels it can be seen that also for well excited modes the damping estimates decrease with increasing noise levels. The reason for this effect can be found in the basic equation of the LSCF method which is shown in equation (20). In order to solve this equation in a least-squares sense, the matrix product $\left[\bar{D}\right]^{\mathrm{H}}\left[\bar{D}\right]$ must be inverted. It was found out that additional white noise improves the condition of that matrix product and thus stabilizes the identification of the complex polynomial coefficients a_i. The effect of the additional noise can therefore be considered as a regularization which is applied to the identification problem. The disadvantages of regularization techniques are well known, namely, that they do not only stabilize an identification process, they can also affect the identification results if the influence of regularization is too strong. For LSCF it can be shown that the imaginary parts of the complex polynomial coefficients a_i identified in equation (20) become small in case of strong regularization (i.e. large noise levels). It is not fully understood, however, why the real parts of the polynomial coefficients remain unaffected. Furthermore, it could not be established why smaller imaginary parts of the complex polynomial coefficients lead to decreasing damping levels of the system poles. From that point of view the study performed here can only state that the damping estimates of LSCF are affected by the noise levels of the FRFs. The damping levels decrease as the noise levels increase and this effect is much more pronounced for poorly excited modes.

Larger errors must be expected for the modal scaling constants (modal mass or modal *"a"*) since the accuracy of these quantities is dependent on the less accurate damping estimates. In particular, the modal scaling constants of poorly excited modes are not reliable since they are affected by the damping estimates of other modes in the current analysis bandwidth as well.

4 Sensitivity with respect to Systematic Errors

The influence of systematic errors will also be studied on the 5-DoF system shown in Figure 2. To this end, the linear arch spring between DoFs 3 and 5 is replaced by an elasto-slip non-linearity to introduce systematic deviations of the (non-linear) FRFs from the linear ones. The elasto-slip non-linearity is a combined stiffness and damping non-linearity whose equivalent mechanical system is shown in Figure 10. It consists of two springs, k_0 and k_1, and a friction element with the normal force f_N and the coefficient of friction μ. In case of harmonic excitation, equivalent non-linear stiffness and damping parameters can be derived which are dependent on the physical parameters k_0, k_1, μ, and f_N, and on the magnitude of the relative displacement response $\Delta u = u_2 - u_1$. In this study, the physical parameters were adjusted in such a way that elasto-slip element has the same underlying linear stiffness (and zero underlying linear damping) as the arch spring which has been replaced. Consequently, the FRFs of very low excitation force levels are equal to the linear FRFs of the original 5-DoF system.

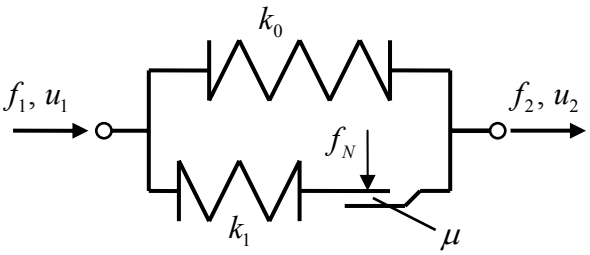

Figure 10: Equivalent mechanical system of the elasto-slip non-linearity

The comparison of the linear and the non-linear acceleration responses (not FRF) obtained at the drive point (DoF 1) when applying a constant excitation force amplitude of 6 N is shown in Figure 11. The non-linear responses shown there were calculated using the (single) Harmonic Balance method. It can be seen that modes 1, 3, and 4 are almost unaffected by the non-linearity, whereas modes 2 and 5 have a combined stiffness- and damping non-linearity. Especially the damping of mode 2 seems to have significantly increased so that in the following the focus will be put on the identification of this mode.

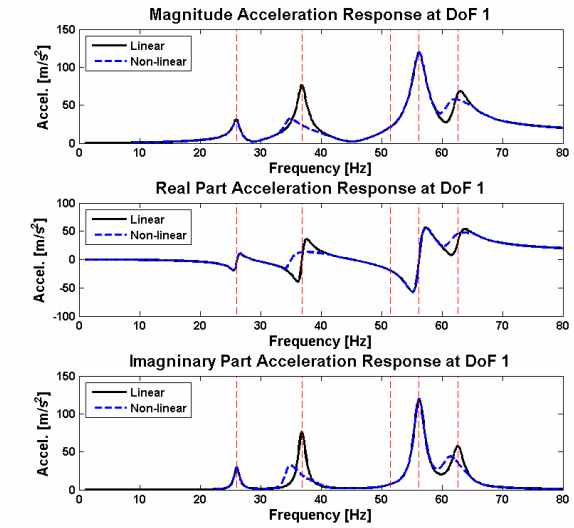

Figure 11: Comparison of linear and non-linear acceleration responses at the drive point

The non-linear FRFs simulated with the 6 N excitation force level were contaminated with a moderate level of noise (15%). Subsequently they were imported into modal analysis software and analyzed using the three methods: FDPI, LSCE, and LSCF. In general, it can be noted that the stabilization diagrams in the case of non-linear data have multiple stable poles at the resonances of those modes which show non-

linear behaviour. This can be observed in Figure 12, where the stabilization diagram obtained with an LSCF type of modal analysis tool is shown and which was obtained with the non-linear FRFs of the 5-DoF system calculated with 6 N excitation force amplitude. The non-linear modes 2 and 5 have multiple stable poles which could not be removed automatically from the stabilization diagram. When all stable poles are retained for mode shape extraction, it can be shown that the stable poles of a certain resonance peak are associated with the same mode shape but have different damping ratios. This makes the selection of meaningful poles more complicated and it is best practice to select a pole which is located directly at the peak frequency, because this frequency is a good estimate for the resonance frequency of that mode at the current response level. The situation can be improved by imposing a low level of artificial noise on the FRFs. As long as the noise level is not too high it stabilizes the pole estimation in the sense of regularization. The identification of multiple stable poles can thus be avoided (at the cost of slightly different damping estimates when using LSCF). This important effect was exploited in case of the non-linear 5-DoF system by introducing a moderate noise level of 15%.

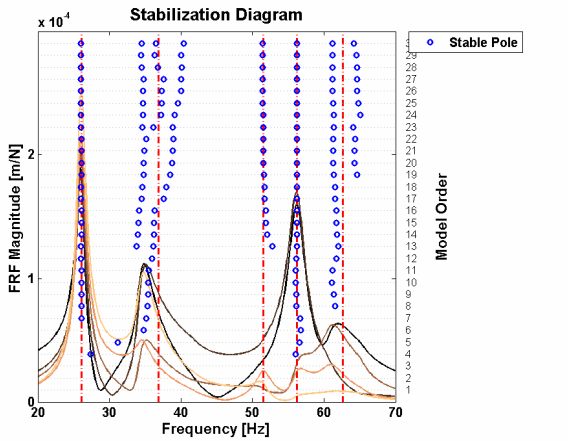

Figure 12: Stabilization diagram obtained with LSCF in case of non-linear FRFs without noise

In the following study, emphasis will be given to the results obtained for mode 2 which is strongly affected by the non-linearity. It can be seen from Figure 11 that the non-linearity is only activated in narrow frequency bands around the resonances of some modes. Therefore, the influence of the analysis bandwidth on the modal parameter estimation was also investigated for each analysis method separately. The results of the modal analysis for mode 2 of the non-linear FRFs of the 5-DoF system are summarized in Table 3. It should be mentioned that the very narrow analysis bandwidth is actually smaller than the bandwidths typically used for modal analysis. Nonetheless, this very narrow bandwidth shall be used here to emphasize the effects which may occur when the bandwidth is narrowed down significantly.

Table 3: Results of modal analysis for mode 2 of the non-linear 5-DoF system

	LSCF		LSCE		FDPI	
Bandwidth	Freq. [Hz]	Damp. [%]	Freq. [Hz]	Damp. [%]	Freq. [Hz]	Damp. [%]
1 to 80	35,34	3,69	34,75	3,74	--	--
20 to 45	35,09	4,06	34,54	4,10	35,29	4,25
31 to 45	34,70	3,76	34,46	3,55	35,01	4,56
33 to 40	34,21	3,48	34,89	1,70	34,64	4,65

It can be seen from Table 3 that the increase of damping and the slightly lower eigenfrequency (compared with the linear system) was detected by all methods. When looking at the LSCF results, it can be seen that the eigenfrequency estimate shifts towards lower frequencies as the analysis bandwidth is narrowed down. The damping estimate of the LSCF method is relatively stable but is generally slightly lower than those of the other methods (except for the very narrow frequency band where LSCE underestimated the damping by far). The LSCE eigenfrequency and damping estimates are relatively independent of the analysis bandwidth. However, if the bandwidth becomes too narrow, LSCE is no longer suitable and results in a

totally wrong damping estimate in the case of the very narrow bandwidth. With FDPI it was not possible to extract mode 2 out of the broad analysis bandwidth from 1 to 80 Hz. From the remaining eigenfrequency and damping estimates it can be seen that the eigenfrequency shifts towards lower frequencies as the analysis bandwidth is narrowed down, whereas the damping estimate increases and is always higher than the other estimates.

It should be mentioned that Table 3 summarizes the results of different modal analysis tools which all tried to fit a linear model to data from a non-linear structure. The results can thus only be equivalent modal parameters which more or less fit the non-linear data. A fundamental feature of non-linear systems is that they do not have constant eigenfrequencies and damping ratios. These quantities are dependent on the response level which develops during the measurements. The responses were calculated analytically and the drive point response is shown in Figure 11 as a function of frequency. When using the calculated responses to evaluate the actual response dependent stiffness and damping values, the actual non-linear modal stiffness and modal damping values can also be obtained as functions of frequency, from which the actual non-linear resonance frequencies and actual non-linear damping ratios can be derived. This is shown in Figure 13, where the actual non-linear resonance frequency and the actual non-linear damping ratio of mode 2 are plotted versus frequency. The non-linear resonance frequency was obtained from the square root of the quotient of the non-linear modal stiffness and the constant modal mass (non-linear Rayleigh quotient). The actual non-linear damping ratio was obtained from the superposition of the underlying linear modal damping and the additional response dependent non-linear modal damping. Modal coupling with other modes due to non-linearity can be observed in Figure 13 by the change of damping and resonance frequency of mode 2 when the excitation frequency approaches the resonance frequencies of other modes.

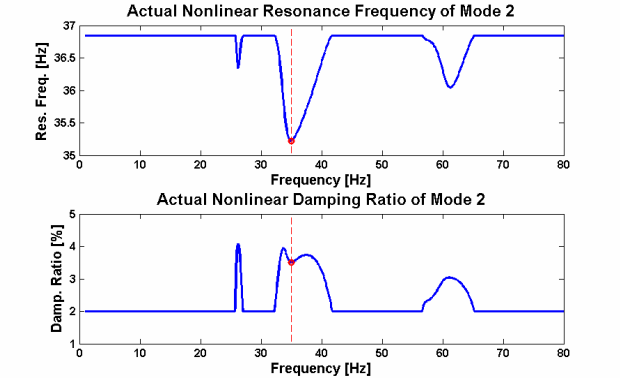

Figure 13: Actual non-linear resonance frequency and damping ratio of mode 2 of the 5-DoF system with elasto-slip non-linearity

The largest response in the vicinity of the resonance of mode 2 of the 5-DoF system shown Figure 11 occurs at 35 Hz. The actual non-linear resonance frequency at this point is 35.23 Hz and the corresponding viscous damping ratio is 3.51%, see Figure 13. These values shall be considered in the following as the "true" non-linear eigenfrequency and damping ratio of mode 2 (related to the 6 N excitation force level). When the modal analysis results summarized in Table 3 are compared with the "true" non-linear eigenfrequency and damping ratio, the quality of the modal analysis of the different methods can be assessed in terms of eigenfrequency- and damping ratio deviation, see Table 4.

Table 4: Eigenfrequency- and damping ratio deviations of non-linear mode 2

	LSCF		LSCE		FDPI	
Bandwidth	**Freq. Dev. [%]**	**Damp. Dev. [%]**	**Freq. Dev. [%]**	**Damp. Dev. [%]**	**Freq. Dev. [%]**	**Damp. Dev. [%]**
1 to 80	0,33	5,13	-1,36	6,55	--	--
20 to 45	-0,40	15,67	-1,96	16,81	0,19	21,08
31 to 45	-1,48	7,12	-2,17	1,14	-0,60	29,91
33 to 40	-2,88	-0,85	-0,96	-51,57	-1,65	32,48

It can be seen from Table 4 that the eigenfrequency estimates obtained with LSCF are quite good, even though they are dependent on the analysis bandwidth. The damping estimated by LSCF is mostly lower than that estimated by the other analysis methods. Nonetheless, it fits better the true non-linear damping than the other methods. LSCE underestimated the eigenfrequency in all cases. The damping estimate failed in the very narrow bandwidth case. The FDPI results are also dependent on the analysis bandwidth. The eigenfrequency decreases and the damping increases when the analysis bandwidth is narrowed down.

The quality of the modal analysis of the non-linear FRFs can only be checked by the synthesis of FRFs with the identified modal parameters. This is shown in Figure 14 to Figure 16 for the 20 to 45 Hz bandwidth. The corresponding stabilization diagrams are shown on the left hand side and the FRF synthesis of the drive point FRF is shown on the right hand side.

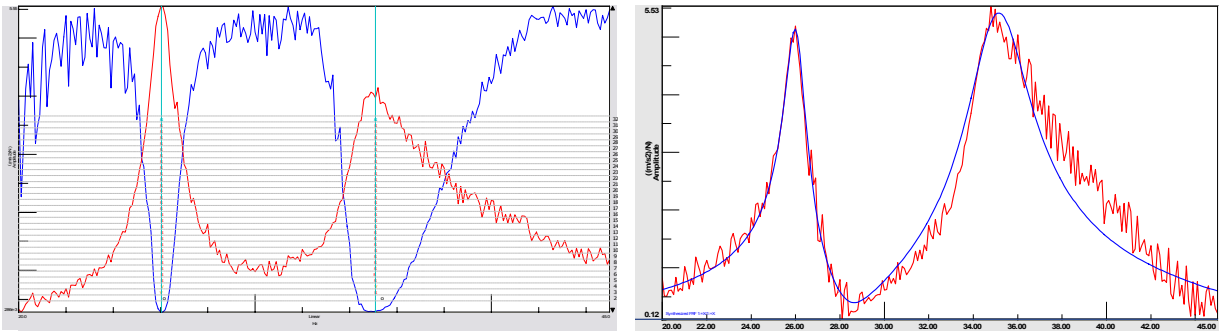

Figure 14: Stabilization diagram and FRF synthesis obtained with LSCF for 20 to 45 Hz bandwidth

It can be seen from Figure 14 that the LSCF stabilization diagram looks very clean. Due to the additional noise on the FRFs the detection of multiple stable poles at a resonance peak of a non-linear mode could be avoided so that two stable poles could be detected in the analysis bandwidth from 20 to 45 Hz. The curve-fit for mode 1 is very good and for mode 2 still acceptable which indicates the quality of the damping estimate.

The LSCE stabilization diagram shown in figure 15 looks quite messy due to the stable computational poles which appear not at the resonance peaks but somewhere between them. These stable computational poles are caused by noise on the FRFs and also by non-linearity. The curve-fit for mode 1 is very good and for mode 2 not as good as the LSCF curve-fit but still not bad. The quality of the damping estimate is therefore considered good but it appears that the eigenfrequency was estimated at a too low frequency.

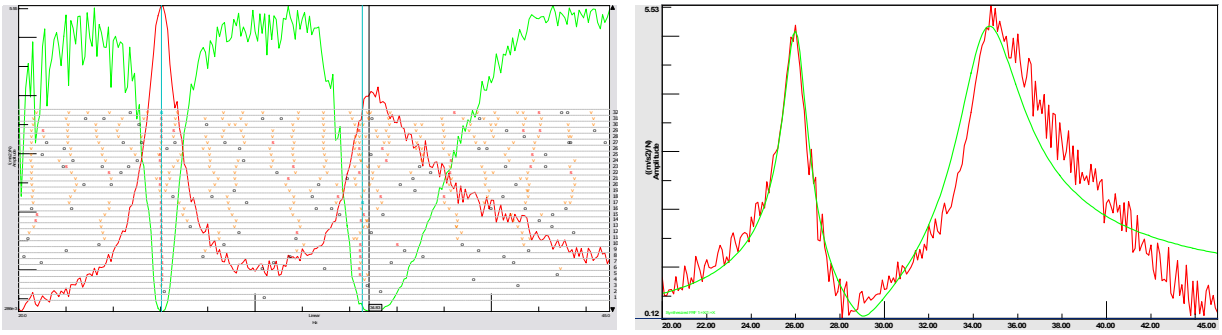

Figure 15: Stabilization diagram and FRF synthesis obtained with LSCE for 20 to 45 Hz bandwidth

The stabilization diagram obtained with FDPI also looks quite messy, see Figure 16, but this feature cannot be related to the noise level. In fact, the stabilization diagram already looked (somewhat less) messy when noise-free non-linear FRFs were analyzed. Nonetheless, FDPI detects two stable poles but the second pole stabilized at too high a frequency. This can be observed in the curve-fit where the resonance peak for mode 2 appears slightly shifted towards higher frequencies. Otherwise the curve-fit looks quite reasonable.

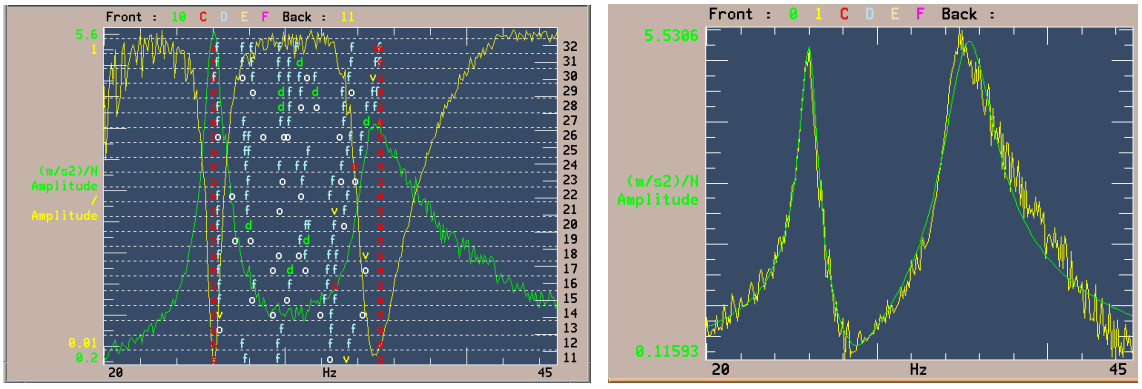

Figure 16: Stabilization diagram and FRF synthesis obtained with FDPI for 20 to 45 Hz bandwidth

As a conclusion of the results of the study of the different modal analysis methods with respect to their sensitivity to systematic errors such as non-linear effects in the FRFs, it should be mentioned that even though modal analysis tools fit a linear model to non-linear data the results are quite acceptable. A dependency of the modal analysis results from the analysis bandwidth was detected and can possibly be used to indicate whether a certain mode is non-linear or not.

The accuracy of the eigenfrequency estimates can be checked by the relative location of the poles to the peak frequencies. The damping estimates are generally less accurate than the eigenfrequency estimates but can be checked by the curve-fit of the synthesized FRFs with the measured ones. If the modal analysis results shall be used for finite element model validation, the damping ratios are typically not required but rather eigenfrequencies and mode shapes. The eigenfrequencies are relatively accurate and also the mode shapes can be extracted from curve-fitting the FRFs with relatively good accuracy (this was not discussed here). Concerning the errors in the modal scaling constants (modal mass or modal *"a"*), the same statement can be made as for the noise-contaminated FRFs: Larger errors must be expected for the modal scaling constants since the accuracy of these quantities is dependent on the less accurate damping estimates. Especially the modal scaling constants of poorly excited modes are not reliable since they are affected by the damping estimates of other modes in the current analysis bandwidth as well.

It should also be mentioned here that only a small analytical system was investigated with a non-linearity which has softening stiffness and increasing damping characteristic. It can be expected (but it has not yet been proved) that the effects observed here appear in a similar way also for other types of non-linearities.

5 Application to Dataset of a Large Aircraft Structure

In this section, the suitability of the different modal analysis methods discussed above will be investigated with respect to the application to data of large aircraft structures. The dataset used for this purpose was acquired during the GVT of the Airbus A380-800 performed in January 2005, see Figure 17 and [6]. A total of 852 sensors were measured, of which 458 were used for modal analysis. FRFs were measured in a frequency range up to 30 Hz using swept-sine excitation with low sweep rates. This type of excitation signal ensures that sufficient energy is associated with each spectral line of the response spectra so that possible non-linearities can be detected from FRF measurements at different excitation force levels.

The data acquired on the A380 show all the features discussed on the analytical 5-DoF system: a significant amount of noise, weakly non-linear behaviour of a few modes and, in addition, a large number of sensors and extremely high modal density. As an example for noise contamination and non-linearity, Figure 18 shows the normalized FRFs which were measured at different excitation force levels in the vicinity of the resonance of a control surface mode. A significant level of noise can be observed and a softening stiffness characteristic with damping levels increasing (note the shift of the eigenfrequency by -20% and the decrease of the amplitude by 60%). This type of non-linearity is similar to the one investigated on the 5-DoF system in section 4.

Figure 17: Ground vibration test of the Airbus A380 (copyright AIRBUS S.A.S.)

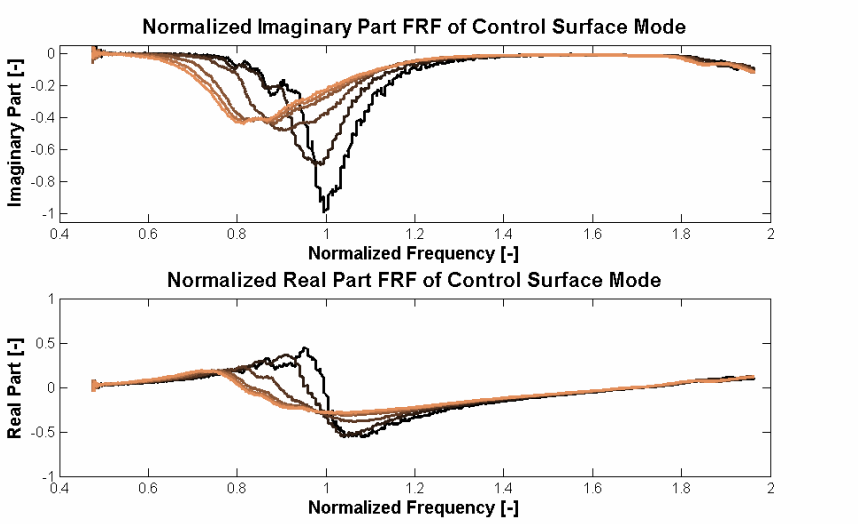

Figure 18: Normalized FRF of a control surface mode measured at different excitation force levels

The complete A380 dataset was analyzed with the LMS Cada-x implementation of FDPI during the GVT. Thus, the FDPI results are considered as the reference solution. Subsequently, the same dataset was analyzed using the LMS Test.Lab implementations of LSCE and PolyMAX (LSCF). From a data handling point of view it must be stated that all methods performed extremely well. Even though the number of sensors (and excitation points) is significantly high, all methods were numerically efficient. In order to check the accuracy of the methods, the results obtained with LSCF and LSCE were compared with the FDPI results. The eigenfrequency deviations of the LSCE and LSCF results of 112 modes are shown in Figure 19. The damping deviations are shown in Figure 20. Limits for the eigenfrequency deviation were set to ±1% and for the damping deviation to ±50% in order to indicate significant differences (note that a damping deviation of 50% still yields a reasonable curve-fit of the FRF according to Figure 9).

The most important statement which can be made is that all modes identified with FDPI could also be identified using LSCF and LSCE. When looking at the LSCF results, it can be seen that 21 modes have a frequency deviation larger than ±1% and only 4 modes deviate more than ±5%. The deviation of damping is more pronounced. In total 27 modes deviate more than ±50% in damping. When looking at the LSCE results, it can again be seen that 21 modes have a frequency deviation larger than ±1%, whereas only 3 modes deviate more than ±5%. 18 modes deviate more than ±50% in damping.

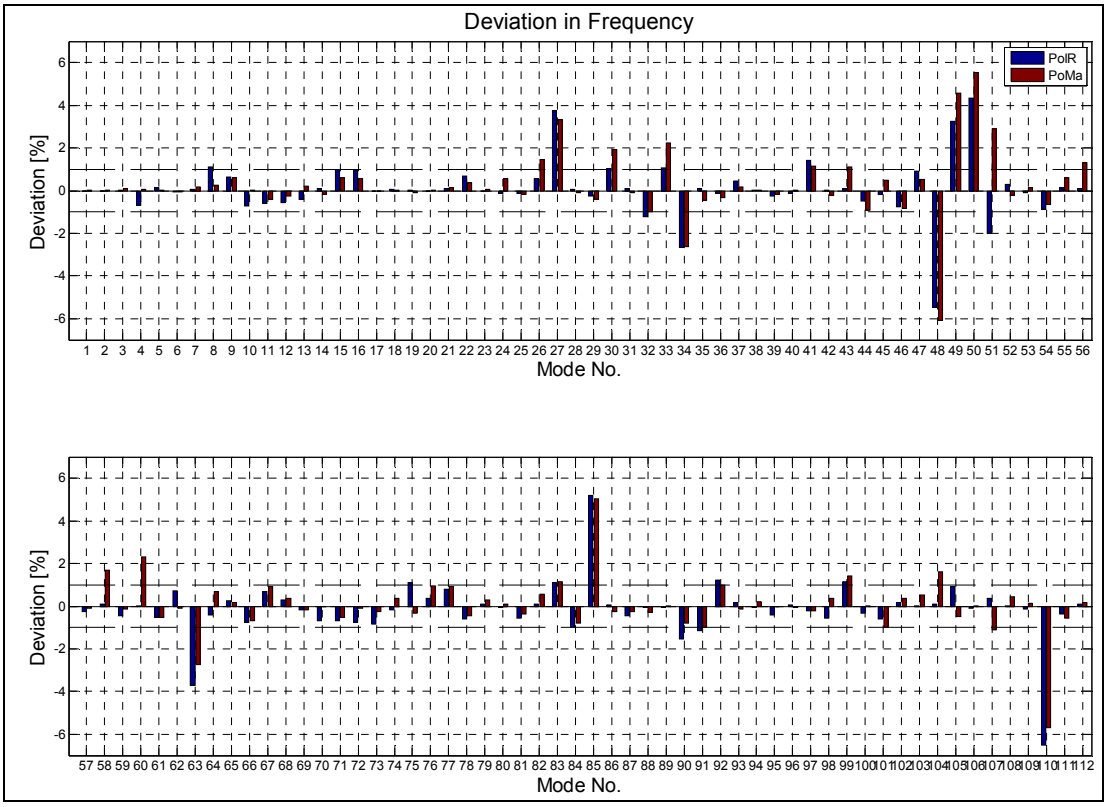

Figure 19: Deviations of the eigenfrequencies obtained with LSCE (PolR) and LSCF (PoMa) with respect to the eigenfrequencies obtained with FDPI

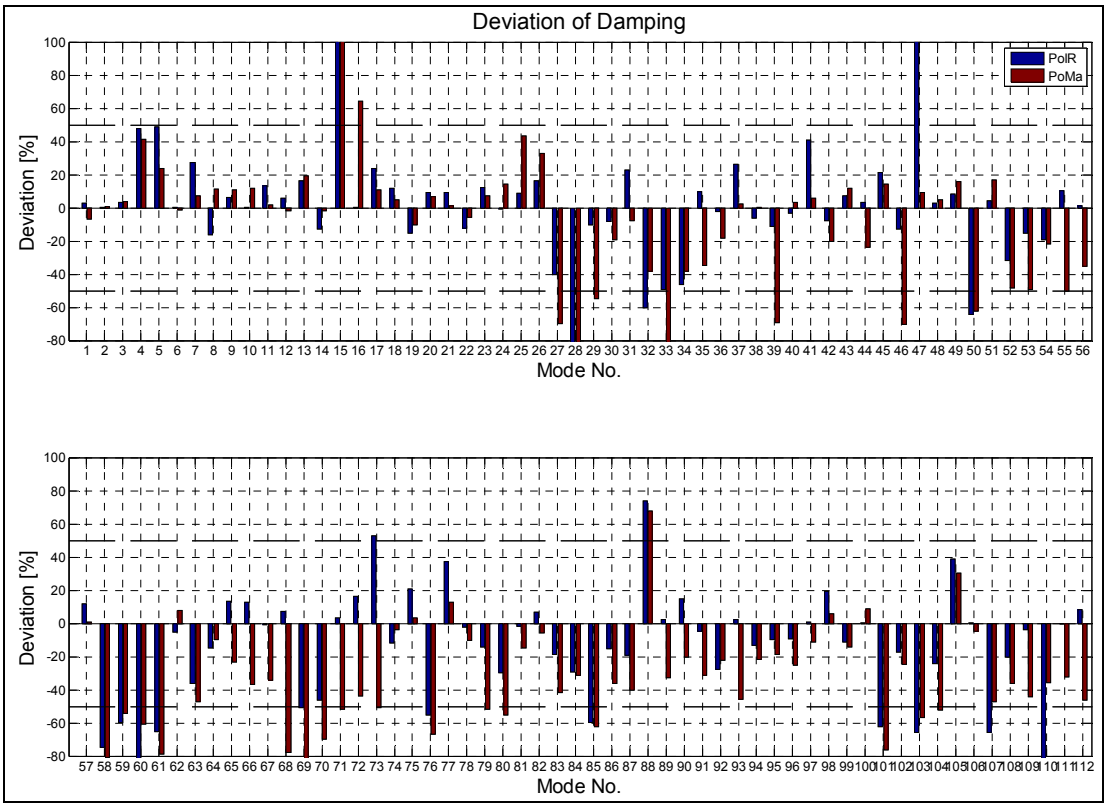

Figure 20: Deviations of the damping ratios obtained with LSCE (PolR) and LSCF (PoMa) with respect to the damping ratios obtained with FDPI

When comparing the results of the different modal analysis methods in terms of eigenfrequencies, no trend is observable regarding an over- or underestimation, see Figure 19. Most of the identified frequencies occur within the limits of ±1% eigenfrequency deviation. Only a few modes show significant deviation. There are two main aspects which are responsible for these larger deviations. First, the selection of the poles is strongly dependent on the operator in case of FDPI and LSCE. Moreover, the stabilization of poles may depend on the analysis bandwidth used for identification. One may also have a larger choice of pole candidates to select which can result in the selection of a computational pole instead of a structural pole, because sometimes computational poles may also yield acceptable curve-fits of the synthesized FRFs. The second reason is the presence of non-linearities which affect the interpretability of the stabilization diagrams. In fact, in most cases with large frequency deviation the control surface were involved and these modes are known to be weakly non-linear, see Figure 18. Depending on the analysis method and on the noise level, the selected poles may vary significantly. The identification processes using the different methods revealed that LSCF yields the most reliable and operator-independent eigenfrequencies.

As mentioned before, all modes identified using the FDPI analysis method were also found using the Test.Lab implementations of LSCF and LSCE. Nevertheless, in some cases significant differences in terms of the MAC correlation were encountered. The main reasons for these deviations are local effects which appear in a different way depending on pole selected from the stabilization diagram. For some modes, only small parts of the aircraft vibrate in phase (local modes) while the rest of the structure vibrates out of phase. When correlating such modes via MAC, the result is worse in any case.

It is conspicuous that LSCF tends to underestimate the damping, and this is also confirmed by the study performed in section 3. When comparing the FDPI identification results with those obtained with LSCF it can be concluded that 74 out of 112 damping parameters were underestimated. Furthermore, when comparing the LSCF results with those of LSCE it can be concluded that 79 damping parameters were underestimated by LSCF. It cannot be concluded here that the damping parameters identified by LSCF are wrong in general. The FRF synthesis should rather be used as the criterion to check the quality/accuracy of the damping estimates and these showed an excellent correlation with the measured FRFs in most cases.

The highest eigenfrequency deviation which can be observed in Figure 19 is likely to be caused by the selection of a computational pole from the FDPI stabilization diagram. For example, mode 110 showed significant eigenfrequency deviation of both methods (LSCF and LSCE) with respect to the FDPI results. It is therefore more likely that the FDPI results are less accurate than the LSCE and LSCF results. This could be confirmed by looking at the stabilization diagrams around mode 110 (which cannot be shown here for reasons of confidentiality). The FDPI stabilization diagram looks totally confusing in this frequency range (which can be a result of noise, non-linearity, or insufficient excitation), whereas the LSCF stabilization diagram shows a single stable pole which slightly drifts towards lower frequencies as the model order is increased. This situation together with the condition that a resonance peak cannot be observed in the sum FRF (and also not in the mode indicator function) can make the selection of a meaningful pole from the stabilization diagram extremely difficult. The result is a mode whose eigenfrequency and damping ratio are highly sensitive to the skills of the operator. In such cases LSCF is the favourable modal analysis tool but it should be kept in mind that this analysis tool does not overcome all problems associated with meaningful pole selection.

6 Summary

Three different modal analysis methods have been discussed in the preceding sections which utilize different representations of the dynamic response function of mechanical structures for modal parameter identification. For example:

- FDPI is derived from a state-space representation of an analytical system and identifies reduced physical system matrices from measured FRFs which are then utilized for analytical modal analysis,

- LSCE performs an inverse Fourier transform on the FRFs and utilizes a time domain representation of the system to extract the poles from impulse response functions,
- LSCF fits a common denominator model to measured FRFs and calculates the system poles from the roots of the complex common denominator polynomial whose polynomial coefficients were identified beforehand from a classical gradient based parameter estimation algorithm.

It can be expected that in some circumstances (i.e. data quality and consistency, presence of non-linearity) certain methods may be preferred over others. At the same time it is extremely difficult to assess from the basic equations which method performs better in certain conditions.

From the results of the studies performed in sections 3 and 4 it can be concluded that LSCE and LSCF can be used for broadband modal analysis, whereas FDPI can sometimes not achieve stability for structural poles when the analysis bandwidth is too broad. FDPI is therefore better suited for narrow band modal analysis. The stabilization diagrams of LSCE are highly sensitive with respect to noise. Additional stable poles appear among the structural poles due to noise and make the stabilization diagrams look somewhat messy. LSCF provides clear stabilization diagrams also in the case of noise-contaminated FRFs. However, the damping estimates associated with the few stable poles decrease with increasing noise levels and this situation becomes worth for poorly excited modes. Since LSCF uses a gradient based parameter estimation algorithm, it is believed that an effect similar to regularization is the cause for this outcome. Eigenfrequencies can be identified from noisy FRFs (and also from non-linear FRFs) with relatively good accuracy. Damping ratios are less accurate and should always be checked by comparing the synthesized FRFs with the measured ones. In cases of non-linear FRFs, it was shown that multiple stable poles can appear at a single resonance peak of a mode which shows non-linear behaviour. These poles are associated with the same mode shape but appear with slightly different frequencies and different damping ratios. This effect makes the selection of meaningful poles difficult. The identification of multiple stable poles for a single resonance peak can be avoided by applying a low level of artificial white noise to the FRFs. Since the effect of noise is similar to regularization it can help to "stabilize" the pole estimation process. The estimates for eigenfrequencies and damping ratios can be dependent on the analysis bandwidth when using FDPI or LSCF. This effect can be exploited for the detection of non-linear modes and can be considered as a practical tool which is readily available in modal analysis software. It was also found out that mode shapes can be extracted from noisy and/or non-linear FRFs with relatively good accuracy. The modal scaling constants (modal mass or modal *"a"*) are sensitive to the damping estimates and are therefore less accurate. This applies in particular for modal scaling constants of poorly excited modes.

The application of the different modal analysis methods to the A380 dataset in section 5 revealed (apart from the efficient data handling and the numerical efficiency which can be attributed to all of them) that all methods are suited for modal analysis of datasets obtained during the GVT of a large aircraft. Even though differences were detected between the results obtained with the different modal analysis tools, these differences could in most cases be explained by physical reasoning and helped to detect advantages and pitfalls in the application of modal analysis tools to datasets which exhibit features like noise, non-linearity, and a large number of FRFs. It can be concluded that it is not sufficient to rely on the results obtained with a single modal analysis tool. The results obtained with different modal analysis tools should rather be checked against each other if the results of modal analysis are suspicious.

7 Acknowledgement

The authors would like to thank Prof. D.J. Ewins from the Imperial College, London, for fruitful discussions during the preparation of the paper. His valuable comments on the scientific subject were gratefully acknowledged.

8 References

[1] G. Gloth, D. Goege: “Handling of Non-Linear Structural Characteristics in Ground Vibration Testing”, International Seminar on Modal Analysis (ISMA), KU Leuven, Belgium, pp. 2129 – 2143, 2004.

[2] LMS International: “The LMS Theory and Background Book – Analysis and Design”, Manual of Test.Lab Revision 5, LMS International, 2005

[3] F. Lembregts: “Frequency Domain Identification Techniques for Experimental Multiple Input Modal Analysis”, Ph. D. Dissertation No. 8803, Dept. of Mechanical Engineering, K. U. Leuven, Belgium, 1988.

[4] D. L. Brown, R. J. Allemang, R. Zimmermann, R. Mergeay: “Parameter Estimation Techniques for Modal Analysis”, SAE Technical Paper Series, No. 790221, 1979

[5] B. Cauberghe: ”Applied Frequency-Domain System Identification in the Field of Experimental and Operational Modal Analysis“, Dissertation, University of Brussels, 2004.

[6] G. Gloth, P. Lubrina: “Ground Vibration Test of the Airbus A380-800”, International Forum on Aeroelasticity and Structural Dynamics (IFASD), Munich, Germany, 2005.